Check for updates

Study on chloride ion resistance durability and mechanism of nano modified concrete sea sand mortar

Wei Fan[1]*, Yingjie Jin[2] and Shengping Wu[1]

[1]Engineering College, Fujian Jiangxia University, Fuzhou, China, [2]College of Civil Engineering, Fuzhou University, Fuzhou, China

This study incorporated nanomaterials to modify traditional sea sand mortar to enhance the durability of marine infrastructure. It explored the effects of nano-silica (NS), nano-metakaolin (NMK), and nano-alumina (NA)) on the chloride binding capacity and microstructure of the sea sand mortar through potentiometric titration, X-ray diffraction (XRD), thermogravimetric analysis (TGA), and scanning electron microscopy (SEM). The results indicated a significant enhancement in the chloride binding capacity of the nanomaterial-modified sea sand mortar. Both NS and NMK reduced Friedel's salt (FS) content in sea sand mortar while enhancing chloride binding capacity via increased physical adsorption. NA increased the FS content in sea sand mortar, thereby enhancing its chemical bonding capacity for chloride ions. Among these three nanomaterials, NMK demonstrated the best improvement in the pore structure of sea sand mortar, followed by NS. The research results provide an innovative material solution for marine engineering structures.

1 Introduction

With the rapid advancement of offshore ports, docks, and maritime engineering projects, the use of sea sand as a substitute for river sand in concrete production can alleviate the shortage of river sand resources while reducing environmental impact. However, direct use of sea sand in construction without desalination treatment may cause corrosion of reinforcing steel bars in concrete structures due to high concentration of chloride ions. This corrosion can substantially compromise the quality and safety of construction projects and adversely affect the durability of reinforced concrete structures. Existing research on the durability of sea sand concrete indicates that chloride ions in cement-based materials are retained via two primary mechanisms: chemical binding and physical adsorption. Chemical binding occurs when chloride ions react with cement hydration phases to form chloroaluminate compounds. Physical adsorption involves the immobilization of chloride ions by hydration products through electrostatic or van der Waals forces (Ting et al., 2020; Hussain and Al-Saadoun, 1992; Suryavanshi et al., 1995; Suryavanshi and Swamy, 1996; Zhang et al., 2021; Chen et al., 2022). Chloride ions present in natural sea sand differ from those introduced by traditional external infiltration and internal incorporation methods. These chloride ions not only adhere to the surface of

the sand particles but also penetrate into their interiors. The release of chloride ions from sea sand involves the dissolution of surface chlorides and the liberation of internal chlorides. Initially, this release is primarily driven by the dissolution of surface chloride ions; once the surface chloride ions have nearly completely dissolved, the liberation of internal chloride ions becomes the primary source. During the early mixing stage of sea sand mortar, surface chloride ions dissolve and come into sufficient contact with the surrounding cement paste, while the relative content of internal chloride ions experiences a rapid increase. As the curing age increases, the internal chloride ions begin to release, with their concentration increasing slowly. Since the pore structure of the mortar has already formed, not all chloride ions can adequately interact with the surrounding binder material, which can impact the solidification of internal chloride ions. Additionally, the precipitation of FS, formed by chemically bound chloride ions, can block the capillary pores in the mortar, making the mortar denser (Yang et al., 2010; Yuan et al., 2009). Therefore, optimizing the pore structure of cement-based materials (CBMs) can prevent or slow down the migration of free chloride ions through the pore solution by disrupting their transport pathways, thereby enhancing the durability of sea sand concrete (Florea and Brouwers, 2012).

Currently, nanomaterials have been extensively utilized in the production of CBMs. Numerous studies have demonstrated that nanomaterials can effectively improve the properties of cement-based materials (Sun et al., 2022; Fan et al., 2014; Ragab, 2019; Liu et al., 2012; Kawashima et al., 2013; Jo et al., 2007; Givi et al., 2010). The mechanisms through which nanomaterials operate in CBMs primarily include the filling effect, chemical effect, and nucleation effect. The filling effect involves nanoparticles filling the pores in CBMs, which increases densification and optimizes pore size distribution, thereby improving mechanical performance. The chemical effect is characterized by the active components in nanomaterials participating in hydration reactions, supplying silica, alumina, and calcium for cement hydration. The nucleation effect is mainly reflected in the provision of nucleation sites for cement hydration products, which facilitates their multi-site growth, thereby enhancing the densification of the matrix (Hou et al., 2020). Ji (2005) indicated that concrete incorporating NS exhibits superior water impermeability and possesses a more uniform and denser microstructure compared to conventional silica-based concrete. They observed that NS particles fill the pores within the C-S-H gel structures and function as nuclei to facilitate strong bonding with C-S-H gel particles, thus improving the durability of the concrete. Said et al. (2012) demonstrated that the addition of NS significantly decreases the average charge and physical penetration depth in concrete, while both total porosity and threshold pore size exhibited significant reductions.

There are limited studies on chloride ion binding capacity of sea sand concrete incorporating nanomaterials. Ragab (2019) suggested that concrete containing nanokaolinite (NMK) exhibits extremely low chloride ion permeability. This was attributed to the reaction between NMK and calcium hydroxide, a byproduct of cement hydration, which generated more C-S-H, C-A-H, and C-A-S-H gels. These gels effectively filled the pore structure, thereby reducing chloride ion permeability. Wang et al. (2019), Yang et al. (2019) indicated that the addition of nano-alumina (NA) helps promote the binding of the calcium sulfoaluminate hydrates (AFm) phase with chloride ions, thereby increasing the solidification of chloride ions. However, further research is essential to determine whether nanomaterials can effectively enhance the chloride ion binding capacity of sea sand concrete and to what extent they improve its microstructure.

Therefore, this study focused on NS, NMK, and NA to systematically investigate the influence of nanomaterials on the properties of sea-sand mortar. X-ray diffraction experiments (XRD) and thermogravimetric analysis (TGA) were conducted to evaluate the differential effects of these nanomaterials on the chloride-ion binding capacity of sea-sand mortar. Scanning electron microscopy (SEM) and mercury intrusion porosimetry (MIP) analyses were employed to explore the impact mechanisms of nanomaterials on the microstructure and pore structure characteristics of sea-sand mortar. Furthermore, grey theory analysis was utilized to establish a quantitative relationship between pore structure parameters and chloride-ion binding capacity (CBC). The overarching goal of this study is to provide robust theoretical insights and practical guidance for the legitimate and sustainable utilization of natural sea sand in construction applications.

2 Materials and methods

2.1 Materials

The main raw materials used in this experiment include sea sand, Portland cement, nano-silica, nano-metakaolin, nano-alumina. The particles of these nanomaterials are characterized by relatively small sizes and a tendency to agglomerate. The particle size distribution and transmission electron microscope (TEM) images are presented in Figure 1, which reveals a lamellae thickness of approximately 20 nm.

The natural sea sand used for the experiment was sourced from the Xiamen sea area, with a fineness modulus of Mx = 2.61, a chloride ion content of 0.079%, and a shell content of 2.53%. The Portland cement meets the current Chinese standard (GB 175–2023) (State Administration for Market Regulation, 2023). The main chemical compositions of hydrophilic nano-silica (NS), nano-alumina (NA) and nano-kaolinite (NMK) are shown in Table 1.

This experiment involves the preparation of cement mortar to investigate the effects of different nanomaterials on the CBC and microstructure of SSM. The water-to-binder ratio was fixed at 0.55, and the binder-to-sand ratio was set at 1:3. Based on the mix proportions outlined in Table 2, the required quantities of raw materials were precisely weighed for use. Subsequently, these materials were sequentially added to a cement mortar mixer and thoroughly blended to achieve a homogeneous slurry. The resulting mixture was poured into cubic molds measuring 70.7 mm × 70.7 mm × 70.7 mm in two layers, followed by vibration compaction and surface smoothing. The molds were removed after resting in a natural environment for 24 ± 2 h and placed in a standard curing room at 20°C ± 3°C with a humidity of RH ≥ 95%.

(a) Particle morphology of sea sand

(b) TEM image of NS

(c) TEM image of NMK
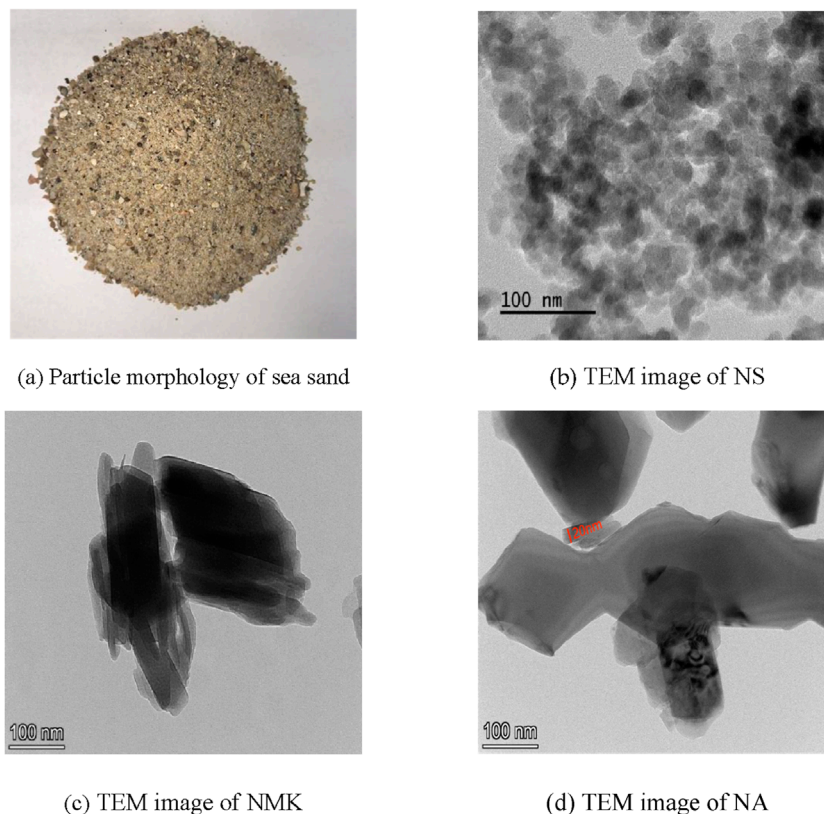
(d) TEM image of NA

FIGURE 1
The morphology of raw materials. **(a)** Particle morphology of sea sand. **(b)** TEM image of NS. **(c)** TEM image of NMK. **(d)** TEM image of NA.

TABLE 1 Chemical composition of raw materials (wt%).

Composition	CaO	SiO2	Al_2O_3	SO_3	Fe_2O_3	MgO	K_2O	TiO_2	Na_2O	P_2O_5
Cement	50.96	26.85	9.15	4.16	3.64	3.16	0.67	0.42	0.34	
NS		96.75	1.15	0.45					1.43	0.01
NMK	0.21	48.27	48.78	0.02	0.52	0.13	0.13	1.18	0.27	
NA		0.10	99.23	0.02	0.01			0.60		

Performance tests were conducted after curing for 3, 7, 28, 56, and 90 days.

2.2 Test method

According to the "Technical specification for test of chloride ion content in concrete" (JGJ/T 322–2013) (Ministry of Housing and Urban-Rural Development of the People's Republic of China, 2021) and "The washed sea sand for construction and municipal engineering" (JG/T 494–2016) (Ministry of Housing and Urban-Rural Development of the People's Republic of China, 2016), the free and total chloride ion contents in the powdered SSM samples were tested using the automatic potentiometric titrator produced

by Mettler Toledo Group. The free chloride ion content (Cf) and total chloride ion content (Ct) in SSM were measured at curing ages of 3, 7, 28, 56, and 90 days. The triplex mortar test blocks were subjected to crushing, random sampling, grinding, and drying in an oven at 105°C ± 5°C until a constant weight was achieved. The samples were subsequently cooled for further use. A powder sample weighing 2 g ± 0.01 g was accurately weighed and transferred into a test tube, followed by the addition of 40 mL deionized water. The test tube was sealed and left undisturbed for 24 h 2 mL of sodium chloride standard solution and 60 mL of deionized water were carefully measured using a pipette and transferred to the sample cup, which was then inserted into the titrator. The titrator automatically recorded the volume of silver nitrate consumed, denoted as V_1. The supernatant of the prepared

TABLE 2 Mixing ratio of nanomaterials modified SSM.

No.	Composition	C (kg/m3)	NS (kg/m3)	NMK (kg/m3)	NA (kg/m3)	W (kg/m3)	SS (kg/m3)	PCE
CN0	Reference group	600				330	1800	0.66
CNS1	Hydrophilic nano-silica modified SSM	594	6	-		330	1800	0.66
CNS3		582	18	-		330	1800	0.66
CNS5		570	30	-		330	1800	0.66
CNMK1	Nano-kaolinite modified SSM	594	-	6		330	1800	0.66
CNMK3		582	-	18		330	1800	0.66
CNMK5		570	-	30		330	1800	0.66
CNA1	Nano-alumina modified SSM	594	-	-	6	330	1800	0.66
CNA3		582	-	-	18	330	1800	0.66
CNA5		570	-	-	30	330	1800	0.66

solution was filtered, while 10 mL of the filtrate and 2 mL of sodium chloride standard solution were transferred into another sample cup. Two drops of phenolphthalein indicator were added to render the solution pink, after which dilute nitric acid was gradually added until the pink color disappeared. Subsequently, 60 mL of deionized water was added, and the sample cup was placed into the titrator for automatic titration. The volume of silver nitrate consumed during this process was recorded as V_2. C_f was automatically calculated using Equation 1.

For the determination of total chloride concentration, another powder sample weighing 2 g ± 0.01 g was accurately weighed and placed in a second test tube. 40 mL of dilute nitric acid (1:7) was added to this sample, and the test tube was sealed and left undisturbed for 24 h. A sample cup was prepared by adding 10 mL of starch solution and 2 mL of sodium chloride standard solution, followed by the addition of 60 mL of deionized water. This sample cup was placed into the titrator for automatic titration. The volume of silver nitrate consumed was recorded as V_1. Next, 10 mL of the solution from the second test tube, 10 mL of starch solution, 2 mL of sodium chloride standardsolution, and 60 mL of deionized water were combined in the sample cup using a pipette, and the titration was repeated. The volume of silver nitrate consumed during this second titration was recorded as V_2. Finally, C_t was calculated according to Equation 1. The chloride binding capacity (CBC) was used to describe the chloride ion binding ability of SSM. It is defined as the ratio of the C_b to the C_t, where the C_b is calculated by subtracting the C_f from the C_t expressed as Equation 2.

$$C = \frac{0.03545 \times C_{AgNO_3} \times (V_2 - V_1)}{m \times \frac{1}{4}} \times 100\% \qquad (1)$$

$$CBC = \frac{C_b}{C_t} = \frac{C_t - C_f}{C_t} \qquad (2)$$

The chemical binding capacity of chloride ions in CBMs is associated with the formation amount of Friedel's salt, while the

physical adsorption capacity of chloride ions is related to the formation amount of C-S-H gel, which in turn depends on the CH content. To examine the phase changes in SSM, the samples that had reached the desired curing age were crushed, and hydration was terminated using isopropanol. They were then dried in a vacuum oven at 50°C for 48 h until a constant weight was achieved. The crushed samples were ground in an agate mortar, and the resulting powder was sieved through a 45 μm brass mesh. The powder was subsequently compacted into square samples on a glass slide.

X-ray diffraction (XRD) analysis was performed for semi-quantitative analysis of the effects of NS, NMK, and NA on the relative content of FS in SSM. This analysis investigated the mechanism by which different nanomaterials affect the CBC from a chemical binding perspective. The testing was conducted over a range of 5°–80°, with a scanning speed of 2°/min and a step size of 0.02°. The qualitative analysis was performed using JADE 9.0 software, while the quantitative analysis of the primary crystalline substances was conducted based on the PDF database.

Thermogravimetric analysis (TG-DTG) tests were conducted using the STA 449F3 synchronous thermal analyzer manufactured by NETZSCH, Germany. The heating rate was set at 10°C/min, with a temperature range of 30°C–1000°C, and nitrogen was used as the protective gas. During the experiment, approximately 10 mg of the sample was weighed and placed into a crucible, while ensuring that the sample did not exceed one-third of the crucible's volume. The TG curve was obtained, and the differential thermogravimetric (DTG) curve was utilized to analyze the weight loss intervals of different phases within the TG curve.

The sample surfaces were gold-coated to investigate the influence of nano-materials on the microstructure and pore structure of sea sand mortar. The microstructural characteristics were analyzed using scanning electron microscopy (SEM). The sample was placed in an expanometer and evacuated to a pressure of less than 6.67 Pa. The specific pore volume and specific surface
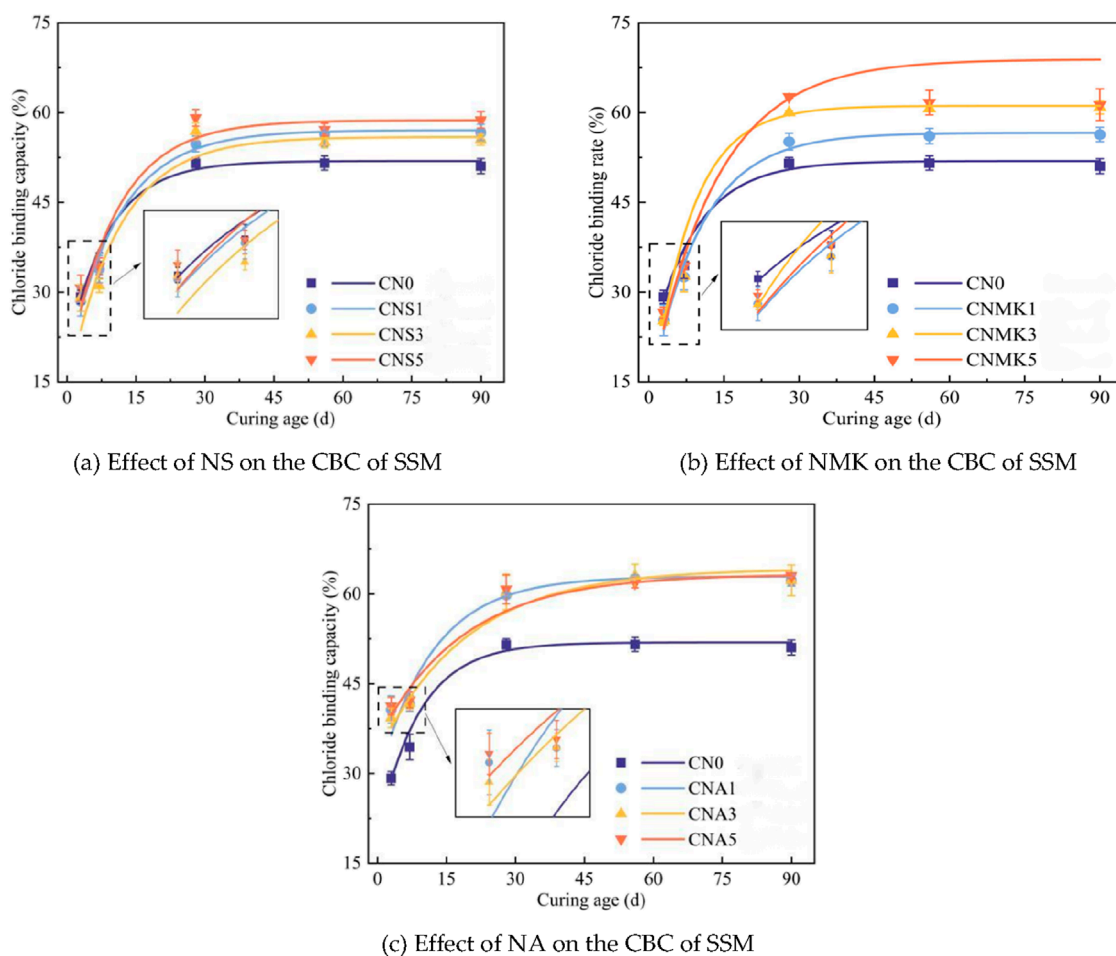
FIGURE 2
Effect of nanomaterials on the CBC of SSM.**(a)** Effect of NS on the CBC of SSM. **(b)** Effect of NMK on the CBC of SSM. **(c)** Effect of NA on the CBC of SSM.

area across different pore size ranges were measured using the computer-controlled mercury intrusion porosimetry (MIP). In the high-pressure range ($0.1655 \leq p \leq 206.843$ MPa), 36 pressure points were selected, with a stabilization duration of 2 s for each point.

3 Results

3.1 Effect of nanomaterials on the CBC of sea sand mortar

3.1.1 Chloride ion potentiometric titration test

Figure 2 illustrates the effects of varying nanomaterial contents on the CBC of SSM.

Figure 2 indicates that the impact of NS on the early CBC of SSM was not significant. At the curing age of 28 days, the CBC of the test groups CNS1, CNS3, and CNS5 increased by 6.32%, 10.42%, and 14.81%, respectively, compared to the control group CN0. In this case, cement hydration was relatively sufficient, and the abundant hydration product, CH, underwent a pozzolanic reaction with NS,

resulting in the formation of additional C-S-H gel. This reaction benefited the enhancement of the CBC of SSM through physical adsorption of chloride ions. As the curing age was extended to 56 and 90 days, minimal changes were observed in the CBC values among the test groups.

At an early curing stage, the three test groups incorporating NMK exhibited reductions in CBC of 13.42%, 13.69%, and 8.94% respectively, compared to the control group CN0. At the curing age of 7 days, the reduction in CBC in these test groups was significantly smaller. This could be attributed to the volcanic ash activity of NMK, which reacted with the cement hydration product CH, resulting in the formation of additional C-S-H gel. Additionally, the aluminum phase present in NMK also contributed to an increase in the chemically bound chloride ion content. At the curing age of 28 days, the CBC values for the test groups increased by 7.07%, 16.45%, and 21.68%, respectively, compared to the control group CN0. At this time, the cement hydration within the system was relatively complete, and the sufficient CH facilitated the pozzolanic reaction with NMK to generate additional C-S-H gel. This process enhanced the physical adsorption of chloride ions by the SSM.

The addition of NA significantly improved the CBC of SSM at all curing stages. At the curing age of 3 days, the CBC values for the groups CNA1, CNA3, and CNA5 increased by 39.31%, 35.54%, and 41.40%, respectively, compared to the control group CN0. At the curing age of 7 days, the CBC values for the groups CNA1, CNA3, and CNA5 increased by 21.15%, 21.25%, and 22.85%, respectively, compared to the control group CN0. When the curing age was further extended to 28 days, the CBC values for the groups CNA1, CNA3, and CNA5 increased by 16.13%, 16.90%, and 18.05%, respectively, compared to the control group. Increasing the NA content from 1 wt% to 5 wt% had a negligible effect on the enhancement of CBC at the same curing stage.

3.1.2 XRD analysis

Figure 3 presents the XRD diffraction patterns of samples CNS5, NMK5, and NA5 at the curing ages of 3, 7, and 28 days, where the marked diffraction peaks for FS, CH, and quartz appear at 11.2°, 18°, and 34.1°, as well as 20.9° and 26.7°, respectively. The presence of FS diffraction peaks in all sample groups suggests that during the curing of SSM samples, the chloride ions dissolved from the surface and released from the interior of the sea sand particles have been chemically bound, thus stabilizing and solidifying within the system. The diffraction peak of FS is not particularly pronounced. This can be attributed to the fact that the amount of chloride bound in the slurry is closely correlated with the concentration of chloride ions within the system. Florea (Ministry of Housing and Urban-Rural Development of the People's Republic of China, 2016) indicated that at a chloride concentration close to that of seawater, the binding percentages of chloride ions by HO-AFm, SO4-AFm, C-S-H gel, as well as FS and Ca(OH)$_2$ were 49%, 20%, 28%, 3% and 0%, respectively. Since C-S-H gel is amorphous, its content cannot be correlated with the intensity of diffraction peaks through XRD analysis (Florea and Brouwers, 2012).

In Figure 3b, no significant shifts in the diffraction peaks of the three types of crystals were observed, suggesting that the incorporation of NMK did not cause noticeable distortion in the formation of internal crystals. The addition of 5 wt% NMK significantly reduced the intensity of the CH diffraction peak in the mortar at the curing age of 28 days. This was attributed to the fact that the active SiO$_2$ and Al$_2$O$_3$ contained in NMK underwent a pozzolanic reaction with CH, which produced additional C-S-H gel that contributes to increasing the compressive strength of the mortar samples. Consequently, the CH content in the mortar system decreased, as reflected by the reduced intensity of CH diffraction peaks.

The incorporation of NA did not reveal any significant new diffraction peaks, suggesting that NA did not lead to the formation of extensive new crystalline materials in the samples. The intensity of the CH diffraction peak in the samples exhibited only a slight decrease at 28 days, which is consistent with the findings of Suryavanshi and Swamy (1996). The partial replacement of cement with NA led to a reduction in CH content; however, its consumption of CH was not very high. The reduction in CH diffraction peak intensity caused by NA in different SSM samples was smaller than that induced by NS and NMK.

3.1.3 TG-DTG analysis

The TG curve reflects the mass changes due to the decomposition of different hydration products at various temperatures. The DTG curve is the first derivative of the TG curve with respect to temperature, and the endothermic peaks at different temperatures correspond to the decomposition of various hydration products. In this experiment, the testing temperature ranged from 30°C to 1,000°C. As depicted in Figure 3, three distinct endothermic peaks were identified in the TG-DTG pattern. They represented the decomposition of three different substances: (1) 100°C–200°C, an endothermic peak due to the dehydration or decomposition of AFt and C-S-H gel; (2) 400°C–500°C, an endothermic peak resulting from the dehydration and decomposition of CH; (3) 550°C–700°C, an endothermic peak resulting from the decomposition of CaCO$_3$, formed by the carbonation of CH, into CO$_2$ shown as Equations 3, 4 (Farzadnia et al., 2013). Additionally, Huang (2014) confirmed through thermogravimetric tests that the weight loss of CBMs containing internally incorporated chloride ions at temperatures between 310°C and 380°C is attributed to the dehydration decomposition of FS. Research by Saikia et al. (2009) indicated that the two main dehydroxylation peaks of FS are located between 100°C–150°C and 230°C–410°C. The former was attributed to the release of four water molecules from the interlayer of the crystal structure, while the latter was associated with the release of six structural water molecules from the main structure of FS.

The weight losses at the endothermic peaks between 400°C–500°C and 550°C–700°C enabled the semi-quantitative calculation of CH generated in SSM samples. This allowed for an assessment of the effects of NS, NMK, and NA on the variation of CH content in SSM. Table 3 presents the relative changes in CH content of the samples at the curing ages of 3, 7, and 28 days.

Due to the overlap in the dehydration ranges of the first four water molecules in C-S-H gel, AFt, and FS, it is challenging to clearly distinguish the relative contents of these substances. Therefore, the weight loss at the endothermic peak between 310°C–380°C was used for the semi-quantitative calculation of the FS content in SSM powder samples. This allowed for the evaluation of the effects of NS, NMK, and NA on the chemical binding capacity of chloride ions in SSM, as detailed in Table 4.

$$Ca(OH)_2 \xrightarrow{heat} CaO + H_2O \tag{3}$$

$$CaCO_3 \xrightarrow{heat} CaO + CO_2 \uparrow \tag{4}$$
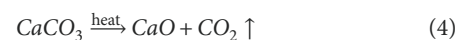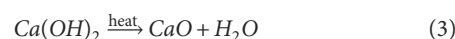
The decomposition amount of calcium hydroxide (CH) is expressed as Equation 5:

$$m_1(CH) = \frac{74}{18} \times \Delta G_1 \tag{5}$$

The carbonization amount of calcium hydroxide (CH) is expressed as Equation 6:

$$m_2(CH) = \frac{74}{44} \times \Delta G_2 \tag{6}$$

The total calcium hydroxide (CH) production is calculated as Equation 7:

$$m(CH) = m_1(CH) + m_2(CH) \tag{7}$$

The amount of FS produced is calculated as Equation 8:

$$m(FS) = \frac{489}{108} \times \Delta G_3 \tag{8}$$
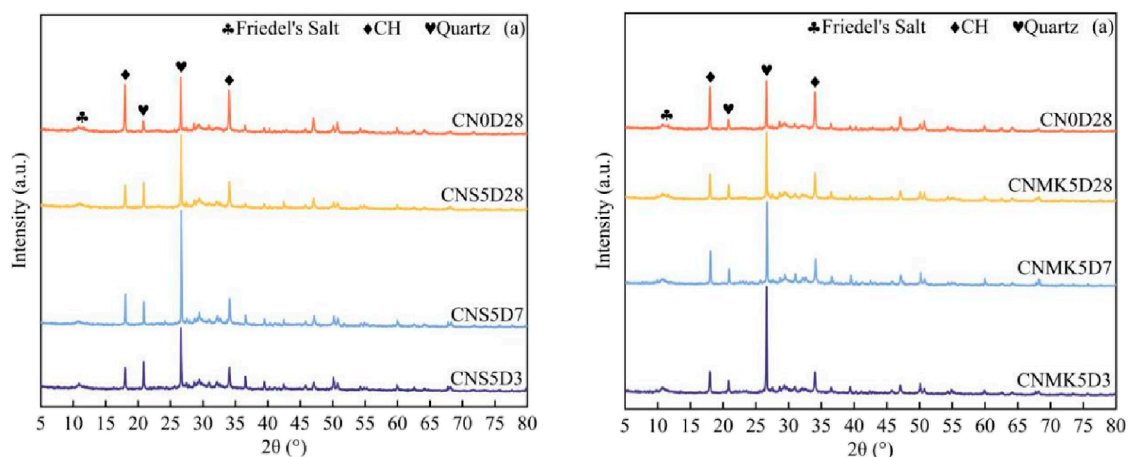
(a) Comparison of the XRD pattern of samples before and after NS modification

(b) Comparison of the XRD pattern of samples before and after NMK modification
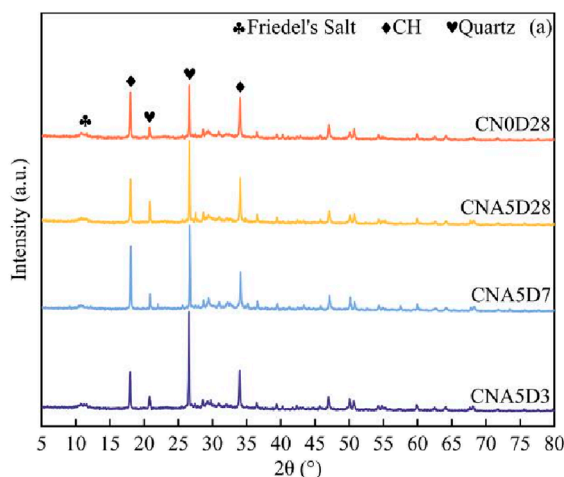
(c) Comparison of the XRD pattern of samples before and after NA modification

FIGURE 3
Comparison of XRD pattern before and after nanomaterial modification. **(a)** Comparison of the XRD pattern of samples before and after NS modification. **(b)** Comparison of the XRD pattern of samples before and after NMK modification. **(c)** Comparison of the XRD pattern of samples before and after NA modification.

TABLE 3 CH contents of samples CNS5, FANS5, and MKNS5 (wt%).

Samples		CN0	CNS5	CNMK5	CNA5
	3 d	11.7	10.7	10.9	11.0
CH content	7 d	20.3	18.1	18.8	19.6
	28 d	17.6	12.5	13.8	16.8

TABLE 4 FS content of samples CNS5, FANS5, and MKNS5 (wt%).

Samples		CN0	CNS5	CNMK5	CNA5
	3 d	5.9	4.8	5.6	6.1
FS content	7 d	5.2	4.8	5.0	5.5
	28 d	4.7	4.2	4.4	4.9

where $\triangle G1$ is the weight loss rate of H_2O in CH, $\triangle G2$ is Weight loss rate of CO_2, $\triangle G3$ is weight loss rate of H_2O in FS, m_1 (CH) is the CH content calculated from the weight loss rate of H_2O produced by the thermal decomposition of CH, m_2 (CH) is the CH content calculated according to the weight loss rate of CO_2 produced by the thermal decomposition of $CaCO_3$, m (CH) is total content of CH, m (FS) is the total FS content, and 18, 44, 74, and 489 are molecular weights of H_2O, CO_2, CH, and FS, respectively, after the loss of 4 water molecules.
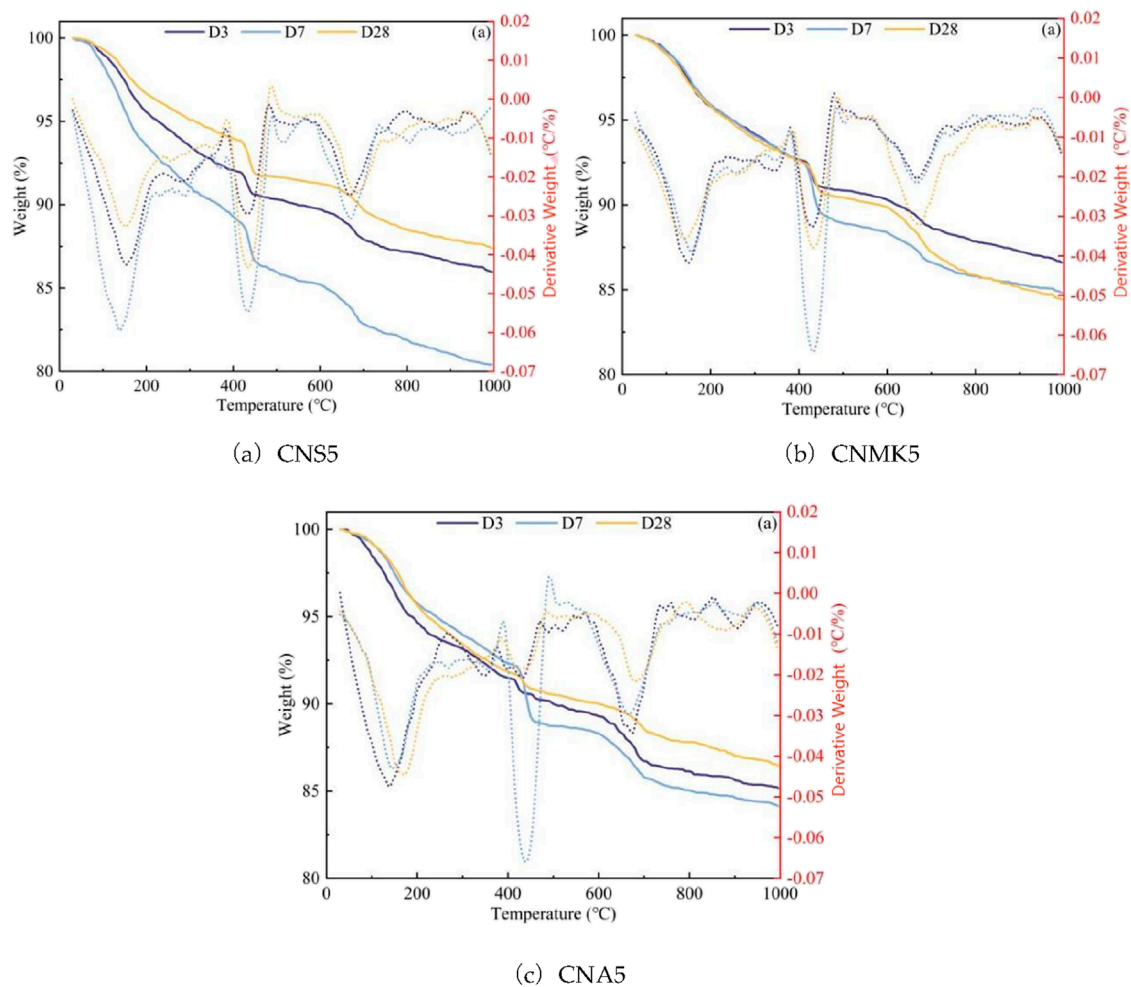
FIGURE 4
TG-DTG pattern of samples CNS5, CNMK5, and CNA5. **(a)**CNS5. **(b)**CNMK5. **(c)**CNA5.

As depicted in Figure 4 and Table 3, the relative content of CH in NS modified SSM at different curing ages was ranked as follows: 7 days >28 days >3 days, which is consistent with the XRD analysis results. This can be attributed to the lower degree of cement hydration at 3 days, resulting in less CH. Additionally, the dissolution of chloride ions from the surface of sea sand and the release of internal chloride ions enabled these ions to chemically react with CH and C_3A to form FS,which further reduced the CH content.

The addition of NMK reduced the relative content of CH in SSM. The relative content of CH in the sample CNMK5 decreased by 6.93%, 7.20%, and 21.47% at the curing ages of 3 days, 7 days, and 28 days, respectively, compared to the sample CN0. This reduction was attributed to the fact that the reactive SiO_2 in NMK chemically reacted with CH to produce additional C-S-H gel, thereby reducing the CH content in the system (Ragab, 2019; Liu et al., 2025). The impact of NMK on reducing the FS content in SSM was less significant than that of NS. This was because NMK contains both reactive SiO_2 and reactive Al_2O_3, and the addition of aluminum phase in the system was beneficial for increasing the FS content. Nevertheless, the replacement of cement with NMK directly led to a reduction in C_3A content. While the aluminum phase in NMK could increase the production of FS, this effect did not sufficiently compensate for the pronounced decrease in FS content due to the reduction in C_3A raw materials caused by the replacement of cement.

The effect of NA on CH content in SSM was less pronounced compared to those of NS and NMK. This may be related to the nucleation effect of NA during the cement hydration process (Shi et al., 2017). Additionally, when NA was added to CBM, it reacted with CH and gypsum in the system, resulting in a further reduction in CH content (Yang et al., 2019). The relative FS content in the sample CNA5 increased by 2.19%, 4.59%, and 4.22% at 3 days, 7 days, and 28 days, respectively, compared to the sample CN0. This further confirmed that the incorporation of NA was beneficial for enhancing the production of FS (Liu et al., 2019). It should be noted that the incorporation of NA hindered the cement hydration reaction, thereby reducing the content of C-S-H gel in the system and decreasing its physical adsorption capacity for chloride ions.

In summary, NS did not enhance the chemical binding capacity for chloride ions in SSM. Instead, the improvement in the CBC due to NS was achieved by increasing the physical adsorption capacity of chloride ions.

3.2 Effect of nanomaterials on the microstructure of SSM

3.2.1 Microscopic morphology of SSM

Due to the porous nature of concrete, there are a large number of pore channels in the interior, which can be used as pathways for chloride ions to flow freely within the concrete. To improve the pore structure, the effect of chloride ions on the durability of cement-based materials can be delayed by reducing the porosity and optimizing the pore size distribution.

Figure 5 presents SEM images of SSM before and after the incorporation of nanomaterials. The incorporation of NS5 and NMK5 resulted in a denser microstructure of SSM. After dispersion treatment, NS was more uniformly distributed in CBMs. Due to its high specific surface energy and pozzolanic activity during hydration, NS could consume CH and undergo secondary hydration reactions. This process generated more C-S-H gel, which contributed to improving the overall density of the structure. Additionally, the hydration products of the cement aggregated around NS, and the uniformly distributed clusters facilitated the formation of a favorable microstructure. The unique size effect of NMK allowed it to effectively fill the pores within the SSM. Moreover, when its active components, SiO_2 and Al_2O_3, dissolved, they could react with the cement hydration product CH to generate additional C-S-H gel or C-A-S-H gel. These gels further filled some of the capillary pores in the matrix, thereby improving the microstructure of the SSM matrix. Figure 5d indicated that the incorporation of NA caused the hydration products, specifically the C-S-H gel within the SSM, to be distributed in the form of "independent" clusters. It is believed that NA affects the normal cement hydration process.

3.2.2 Pore structure of SSM

Table 5 presents the MIP analysis results of the samples. Based on the impact of pore size on strength, the pores in concrete were classified into four categories: harmless pores (d ≤ 20 nm), less harmful pores (20 nm < d ≤ 50 nm), harmful pores (50 nm < d ≤ 200 nm), and more harmful pores (d > 200 nm) (Wu, 1999).

Table 5 indicated that the addition of NS improved the pore structure of SSM. Compared to the control group, the sample CNS5 showed a decrease of 31.76% and 38.78% in more harmful and harmful pores, respectively, while the less harmful and harmless pores increased by 35.62% and 53.43%, respectively, resulting in a 4.08% reduction in porosity. The incorporation of NS significantly reduced the most probable pore diameter in SSM. The improvement in the pore structure due NS was attributed to its small size effect, which allowed it to effectively fill the micro-pores in CBMs, thereby decreasing the porosity and increasing the density.

In comparison to the control group, the CNMK5 sample showed a reduction of 38.47% and 33.64% in more harmful and harmful pores, respectively, while less harmful and harmless pores increased by 20.02% and 64.12%, respectively. The porosity decreased by 9.94%. The addition of NMK significantly reduced the most probable pore diameter in SSM to 5.1685 nm.

The improvement in the pore structure by NMK was mainly attributed to the following reasons (Behfarnia and Salemi, 2013; Zhan et al., 2020). (1) Filling effect: The sheet size of NMK is approximately 1/1,000 of the average size of cement particles (20 μm), which allowed it to act as a filler to occupy the microstructural pores in CBMs. (2) Pozzolanic reaction: NMK could react with the hydration product CH of cement to generate additional C-S-H gel. (3) Nucleation effect: NMK provided a prefabricated nucleus for cement hydration, which allowed C-S-H gel to continuously grow on this nucleus. NMK and NS shared a similar mechanism in enhancing the pore structure of CBMs. Nonetheless, data suggested that NMK achieved a more pronounced improvement in the pore structure.

For the sample CNA5, the percentages of more harmful and harmful pores decreased by 6.30% and 31.06%, respectively, while the percentages of less harmful and harmless pores increased by 17.67% and 22.11%. However, its porosity increased by 1.10%. The incorporation of NA significantly reduced the most probable pore diameter in SSM. The filling effect of NA effectively reduced the porosity of SSM. However, analysis from previous compressive strength tests indicated that this reduction in porosity did not lead to an increase in compressive strength. Farzadnia et al. (2013) demonstrated through differential scanning calorimetry (DSC) testing that the addition of NA resulted in the formation of defective CH. This could lead to stress concentration points within the CBMs, making SSM more prone to cracking and failure during load testing, which in turn manifested as a reduction in compressive strength.

3.2.3 Analysis of grey correlation degree

The grey correlation analysis method is an evaluation method to assess the correlation degree of each factor according to the similarity of the development trend of each factor. It can quantify the relative changes between the various factors, and there is no strict rule on the number of samples. Therefore, the grey correlation degree was used in this experiment to analyze the correlation between pore structure characteristic parameters and chloride ion binding capacity of sea sand mortar before and after NS, NMK, and NA modification.

The sub-sequences were set as harmless pore porosity, less harmful pore porosity, harmful pore porosity, multi-harmful pore porosity, total porosity, most available pore size and fractal dimension, which were x1, x2, x3, x4, x5, x6, and x7, respectively, and the parent sequence y is the 28-day chloride ion curing rate. The grey correlation analysis was performed according to the following steps:

The subsequence was treated dimensionless to get the mean image expressed as Equations 9, 10:

$$\overline{x_j} = \frac{1}{n} \sum_{k=1}^{n} x_j, j = 1, 2, \ldots, m \tag{9}$$

$$x'_{ij} = \frac{x_{ij}}{\overline{x_j}}, i = 1, 2, \ldots, n; j = 1, 2, \ldots, m \tag{10}$$

The parent sequence was treated dimensionless to obtain the mean image expressed as Equations 11, 12:

$$\overline{y} = \frac{1}{m} \sum_{k=1}^{m} y \tag{11}$$
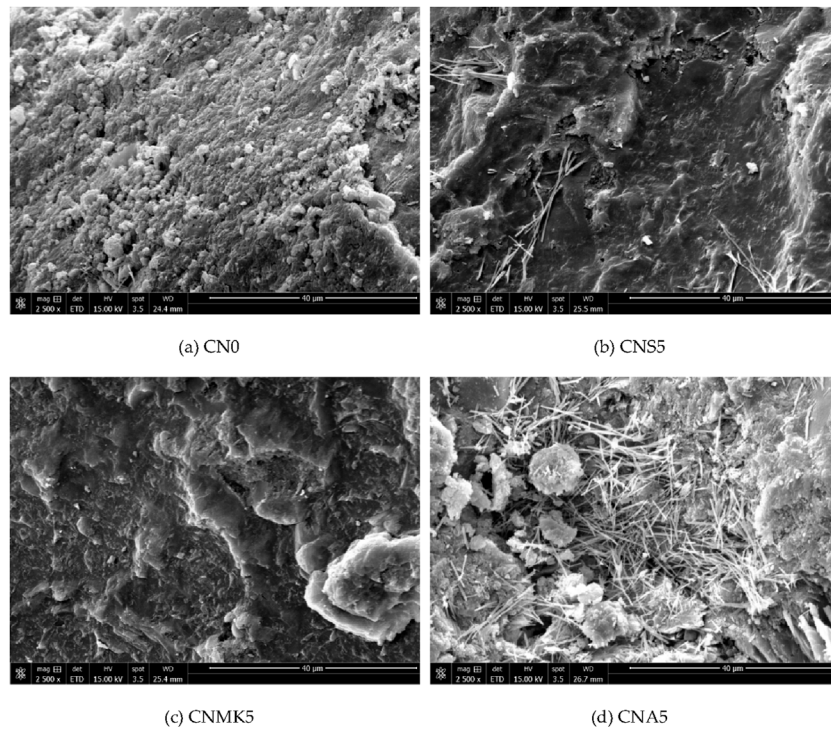
FIGURE 5
Comparison of SEM images before and after modification. **(a)** CN0. **(b)** CNS5. **(c)** CNMK5. **(d)** CNA5.

TABLE 5 Effect of nanomaterials on the pore size distribution of SSM.

Samples	Porosity(%)	Fractal dimension	Most probable pore size (nm)	Pore size distribution (%)			
				Harmless pore	Less-harmful pore	Harmful pore	More-harmful pore
CN0	19.1	2.6	62.5	30.5	10.64	19.8	39.0
CNS5	18.3	2.6	5.2	46.8	14.4	12.1	26.6
CNMK5	17.2	2.6	5.2	50.0	12.8	13.2	24.0
CNMK5	17.2	2.6	5.2	50.0	12.8	13.2	24.0

$$y_i' = \frac{y_i}{\bar{y}}, i = 1, 2, \ldots, n \tag{12}$$

The absolute value between the subsequence and the parent sequence was determined as Equation 13:

$$\Delta_{ij} = \left| y_i' - x_{ij}' \right|, i = 1, 2, \ldots, n; j = 1, 2, \ldots, m \tag{13}$$

The maximum A and minimum B of the sequence difference were determined as Equations 14, 15:

$$A_j = \max\left(\Delta_{1j}, \Delta_{2j}, \ldots, \Delta_{nj}\right), j = 1, 2, \ldots, m \tag{14}$$

$$B_j = \min\left(\Delta_{1j}, \Delta_{2j}, \ldots, \Delta_{nj}\right), j = 1, 2, \ldots, m \tag{15}$$

The correlation coefficient was calculated as Equation 16:

$$\alpha_{ij} = \frac{B_j + \beta A_j}{\Delta_{ij} + \beta A_j}, i = 1, 2, \ldots, n; j = 1, 2, \ldots, m \tag{16}$$

where β is the resolution coefficient, with a value of 0.5.

The correlation degree was calculated as Equation 17:

$$\alpha_j' = \frac{1}{n} \sum_{i=1}^{n} \alpha_{ij}, i = 1, 2, \ldots, n; j = 1, 2, \ldots, m \tag{17}$$

To study the correlation between the pore structure characteristic parameters of NS, NMK, and NA modified sea sand mortar and the 28-day chloride ion curing rate, the sub-sequences were set as harmless pore porosity, low-damage pore porosity, harmful pore porosity, multi-damage pore porosity, total porosity,

TABLE 6 Subsequence and parent sequence.

No.	Porosity of harmless pores x1	Porosity of less-harmful Pore x2	Porosity of harmful pore x3	Porosity of more-harmful Pore x4	Total porosity x5	Most probable pore size x6	Fractal dimension x7	Chloride binding capacity y1
1	5.8	2.0	3.8	7.5	19.1	62.5	2.6	51.5
2	8.6	2.7	2.2	4.9	18.3	5.2	2.6	59.1
3	6.8	1.9	3.1	6.5	18.3	5.2	2.7	48.7
4	11.5	1.1	0.5	4.7	17.8	4.0	2.6	63.5

TABLE 7 Correlation analysis.

Porosity of harmless pores x1	Porosity of less-harmful pore x2	Porosity of harmful pore x3	Porosity of more-harmful pore x4	Total porosity x5	Most probable pore size x6	Fractal dimension x7
0.59	0.71	0.57	0.53	0.61	0.61	0.50

most available pore size and fractal dimension, which were x1, x2, x3, x4, x5, x6, and x7, respectively. The parent sequence y2 is the 28-day chloride ion curing rate, as shown in Table 6.

The correlation degree between pore structure characteristic parameters and chloride ion binding rate was calculated according to the formulas, and the results are shown in Table 7. It shows the relationship between the various porosity and fractal dimensions and the 28-day chloride binding rate. The order of the grey correlation degree is as follows: porosity of least damaged hole > most available pore size > total porosity > Porosity of harmless hole > porosity of harmful pores > porosity of multi-damaged pores > fractal dimension. Among the pore structure characteristic parameters, the porosity of low-damage pores has the highest correlation with the 28-day chloride ion binding rate of sea sand mortar, indicating that pores with a diameter of 20 nm < d ≤ 50 nm have the greatest impact on the improvement of compressive strength of sea sand mortar. The correlation between the fractal dimension and the 28-day chloride ion binding rate is relatively lowest, and the fractal dimension reflects the complexity of the pore structure. It is believed that increasing the complexity of the pore structure can slow down the free movement of chloride ions in the internal pores of the cement-based materials, and then reduce the contact between chloride ions and the cementable materials, which has little influence on the solidification of chloride ions in the system.

4 Discussion

Replacing traditional river sand with sea sand in concrete preparation is crucial for reducing carbon emissions, addressing river sand scarcity, and minimizing environmental impact. Despite the relatively high initial input cost of nano-silica, a comprehensive analysis of the entire life cycle of concrete structure indicates that

its performance enhancement, service life extension, and reduction in maintenance and replacement needs yield significant economic benefits. During this project's experimental research, several areas need further exploration: (1) While the study analyzed Friedel's salt generation under various factors, it did not quantify C-S-H gel formation. Future studies should analyze both compounds, distinguishing chemical binding from physical adsorption during chloride ion binding. (2) To investigate the influence of nanomaterials on the microstructure and their interactions with the hydration products of cement, a mortar system was selected due to its relative simplicity compared to that of concrete systems. This choice facilitates a more precise analysis of the mechanisms by which nanomaterials function. Subsequently, further tests can be conducted on nano-modified concrete to acquire more comprehensive data on material performance. (3) The study focused on nanomaterials' influence on chloride ions but did not assess their impact on steel bar corrosion. Future work could examine embedded steel bar corrosion behavior, providing valuable insights for practical engineering applications.(4) When nanomaterials are introduced into the marine environment, they undergo a series of physical, chemical, and biological transformations due to the complex nature of the oceanic ecosystem (including seawater composition, pH levels, temperature, light conditions, and biological activities, among others). These transformations significantly influence the migration.thereby affecting ecological risks and environmental fate. It iIt is necessary to conduct further research on the transformation mechanism of nanomaterials in the ocean.

5 Conclusion

Chloride ion potentiometric titration tests were conducted to investigate the effects of NS, NMK, and NA on the CBC of

SSM. These findings were further supported by XRD and TD-DTG analyses to elucidate the underlying mechanisms. The main conclusions are as follows: (1) NS, NMK, and NA all contribute to enhancing the chloride ion curing capacity of sea sand mortar. While the influence of NS on the early-stage chloride ion curing amount in sea sand mortar is relatively limited, it demonstrates a pronounced improvement effect during this later stages. NS enhances the chloride ion curing rate of sea sand mortar at all ages, with a significant increase observed at varying dosages. Based on the existing research conducted by our group, NS and NA are identified as the most suitable materials for improving the chloride ion curing capacity of sea sand mortar when kaolin is used as the supplementary cementitious material, with an optimal dosage of 5 wt%. NMK reduces the early-stage chloride ion curing rate in sea sand mortar but significantly improves the curing rate during the later stages. NMK is the most suitable material for enhancing the chloride ion curing capacity of sea sand mortar when fly ash serves as the supplementary cementitious material, with an optimal dosage of 5 wt%. (2) Through XRD and DTG test analyses, it can be concluded that the incorporation of NS, NMK, and NA all reduce the relative content of $Ca(OH)_2$ in sea sand mortar. NS and NMK decrease Friedel's salt in various systems of sea sand mortar; thereby reducing the chemical binding effect of the system on chloride ions. The enhancement of chloride ion curing capacity by NS and NMK is achieved through improved physical adsorption of chloride ions. In contrast, NA increases the relative content of Friedel's salt in sea sand mortar, enhancing the chloride ion curing capacity by increasing the chemical binding amount of chloride ions.

Data availability statement

The raw data supporting the conclusions of this article will be made available by the authors, without undue reservation.

Author contributions

WF: Conceptualization, Data curation, Project administration, Validation, Writing – original draft, Writing – review and editing. YJ: Data curation, Investigation, Writing – original draft. SW: Investigation, Methodology, Writing – review and editing.

Funding

Conflict of interest

The authors declare that the research was conducted in the absence of any commercial or financial relationships that could be construed as a potential conflict of interest.

Generative AI statement

The author(s) declare that no Generative AI was used in the creation of this manuscript.

Publisher's note

All claims expressed in this article are solely those of the authors and do not necessarily represent those of their affiliated organizations, or those of the publisher, the editors and the reviewers. Any product that may be evaluated in this article, or claim that may be made by its manufacturer, is not guaranteed or endorsed by the publisher.

References

Behfarnia, K., and Salemi, N. (2013). The effects of nano-silica and nano-alumina on frost resistance of normal concrete. *Constr. Build. Mater.* 48, 580–584. doi:10.1016/j.conbuildmat.2013.07.088

Chen, L., Li, S., Zhang, H., Huang, C., and Chen, D. (2022). Investigation on mechanism and model of chloride dissolution from sea sand. *J. Hohai Univ.* 50 (03), 104–109. doi:10.3876/j.issn.1000-1980.2022.03.014

Fan, Y., Zhang, S., Kawashima, S., and Shah, S. P. (2014). Influence of kaolinite clay on the chloride diffusion property of cement-based materials. *Cem. Concr. Compos.* 45 (1), 117–124. doi:10.1016/j.cemconcomp.2013.09.021

Farzadnia, N., Ali, A. A. A., and Demirboga, R. (2013). Characterization of high strength mortars with nano alumina at elevated temperatures. *Cem. Concr. Res.* 54, 43–54. doi:10.1016/j.cemconres.2013.08.003

Florea, M. V. A., and Brouwers, H. J. H. (2012). Chloride binding related to hydration products: Part I: ordinary Portland Cement. *Cem. Concr. Res.* 42 (2), 282–290. doi:10.1016/j.cemconres.2011.09.016

Givi, A. N., Rashid, S. A., Aziz, F. N. A., and Sallen, M. A. M. (2010). Experimental investigation of the size effects of SiO2 nano-particles on the mechanical properties of binary blended concrete. *Compos. Part B Eng.* 41 (8), 673–677. doi:10.1016/j.compositesb.2010.08.003

Hou, P., Shi, J., Prabakar, S., Cheng, X., Wang, K., Zhou, X., et al. (2020). Effects of mixing sequences of nanosilica on the hydration and hardening properties of cement-based materials. *Constr. Build. Mater.* 263, 120226. doi:10.1016/j.conbuildmat.2020.120226

Huang, T. (2014). *The influence and mechanism of trace chemical admixtures on the strength of Portland cement [dissertation/Doctor's thesis]. [Beijing(IL)]*. Beijing: China University of Mining and Technology.

Hussain, S. E., and Al-Saadoun, S. S. (1992). Effect of tricalcium aluminate content of cement on chloride binding and corrosion of reinforcing steel in concrete. *Aci Mater. J.* 89 (1), 3–12. doi:10.14359/1239

Ji, T. (2005). Preliminary study on the water permeability and microstructure of concrete incorporating nano-SiO2. *Cem. Concr. Res.* 35 (10), 1943–1947. doi:10.1016/j.cemconres.2005.07.004

Jo, B. W., Kim, C. H., Lim, J. H., and Park, J. B. (2007). Characteristics of cement mortar with nano-SiO2 particles. *Constr. Build. Mater.* 21 (6), 1351–1355. doi:10.1016/j.conbuildmat.2005.12.020

Kawashima, S., Hou, P., Corr, D. J., and Shah, S. P. (2013). Modification of cement-based materials with nanoparticles. *Cem. Concr. Compos.* 36, 8–15. doi:10.1016/j.cemconcomp.2012.06.012

Liu, X., Chen, L., Liu, A., and Wang, X. (2012). Effect of nano-CaCO3 on properties of cement paste. *Energy Procedia* 16 (1), 991–996. doi:10.1016/j.egypro.2012.01.158

Liu, X., Ma, B., Tan, H., Li, H., Mei, J., Zhang, T., et al. (2019). Chloride immobilization of cement-based material containing nano-Al2O3. *Constr. Build. Mater.* 220, 43–52. doi:10.1016/j.conbuildmat.2019.05.148

Liu, Y., Wu, W. Z., Zhang, Y. X., Hou, W., Zhang, H., and Peng, L. G. (2025). Engineered/strain-Hardening cementitious composites (ecc/SHCC) for resilient cold-region infrastructure: a critical review of freeze-thaw durability. *Case Stud. Constr. Mater.* 22, e04362. doi:10.1016/j.cscm.2025.e04362

Ministry of Housing and Urban-Rural Development of the People's Republic of China (2016). *Purified Sea sand for construction and municipal engineering*. Beijing: China building industry press.

Ministry of Housing and Urban-Rural Development of the People's Republic of China (2021). *Technical specification for detection of chloride ion content in concrete*. Beijing: China building industry press.

Ragab, A. E. R. (2019). Physico-chemical properties of nano metakaolin on the characteristics of blended limestone cement. *J. Build. Pathology Rehabilitation* 4 (1), 9. doi:10.1007/s41024-019-0048-6

Said, A. M., Zeidan, M. S., Bassuoni, M. T., and Tian, Y. (2012). Properties of concrete incorporating nano-silica. *Constr. Build. Mater.* 36, 838–844. doi:10.1016/j.conbuildmat.2012.06.044

Saikia, N., Kato, S., and Kojima, T. (2006). Thermogravimetric investigation on the chloride binding behaviour of MK–lime paste. *Thermochim. Acta* 444 (1), 16–25. doi:10.1016/j.tca.2006.02.012

Shi, Z., Geiker, M. R., Lothenbach, B., Weerdt, K. D., Garzón, S. F., Enemark-Rasmussen, K., et al. (2017). Friedel's salt profiles from thermogravimetric analysis and thermodynamic modelling of Portland cement-based mortars exposed to sodium chloride solution. *Cem. Concr. Compos.* 78, 73–83. doi:10.1016/j.cemconcomp.2017.01.002

State Administration for Market Regulation (2023). *Common Portland cement.* Beijing: Standards Press of China.

Sun, J., Shi, Z., Dai, J., Song, X., and Hou, G. (2022). Early hydration properties of Portland cement with lab-synthetic calcined stöber nano-SiO2 particles as modifier. *Cem. Concr. Compos.* 132, 104622. doi:10.1016/j.cemconcomp.2022.104622

Suryavanshi, A. K., Scantlebury, J. D., and Lyon, S. B. (1995). The binding of chloride ions by sulphate resistant Portland cement. *Cem. Concr. Res.* 25 (3), 581–592. doi:10.1016/0008-8846(95)00047-G

Suryavanshi, A. K., and Swamy, R. N. (1996). Stability of Friedel's salt in carbonated concrete structural elements. *Cem. Concr. Res.* 26 (5), 729–741. doi:10.1016/S0008-8846(96)85010-1

Ting, M. Z. Y., Wong, K. S., Rahman, M. E., and Joo, M. S. (2020). Mechanical and durability performance of marine sand and seawater concrete incorporating silicomanganese slag as coarse aggregate. *Constr. Build. Mater.* 254, 119195. doi:10.1016/j.conbuildmat.2020.119195

Wang, Y., Shui, Z., Gao, X., Huang, Y., Yu, R., and Xiao, X. (2019). Modification on the chloride binding capacity of cementitious materials by aluminum compound addition. *Constr. Build. Mater.* 222, 15–25. doi:10.1016/j.conbuildmat.2019.06.137

Wu, Z. (1999). *High performance concrete*. Beijing: China Railway Publishing House, 22–24.

Yang, E. I., Kim, M. Y., Park, H. G., and Yi, S. T. (2010). Effect of partial replacement of sand with dry oyster shell on the long-term performance of concrete. *Constr. Build. Mater.* 24 (5), 758–765. doi:10.1016/j.conbuildmat.2009.10.032

Yang, Z., Gao, Y., Mu, S., Chang, H., Sun, W., and Jiang, J. (2019). Improving the chloride binding capacity of cement paste by adding nano-Al2O3. *Constr. Build. Mater.* 195, 415–422. doi:10.1016/j.conbuildmat.2018.11.012

Yuan, Q., Shi, C., Schutter, G. D., Audenaert, K., and Deng, D. (2009). Chloride binding of cement-based materials subjected to external chloride environment-A review. *Constr. Build. Mater.* 23 (1), 1–13. doi:10.1016/j.conbuildmat.2008.02.004

Zhan, P. M., He, Z. H., Ma, Z. M., Liang, C. F., Zhang, X. X., Abreham, A. A., et al. (2020). Utilization of nano-metakaolin in concrete: a review. *J. Build. Eng.* 30, 101259. doi:10.1016/j.jobe.2020.101259

Zhang, Y., Zheng, S., Sun, L., Long, L., Yang, W., and Li, L. (2021). Developing GIS-based earthquake loss model: a case study of Baqiao District, China. *Bull. Earthq. Eng.* 19, 2045–2079. doi:10.1007/s10518-020-01039-z